DOI: 10.1002/ ((please add manuscript number))
Article type: Full Paper

Unveiling the Dynamic Processes in Hybrid Lead Bromide Perovskite Nanoparticle Thin Film Devices

Bianka M. D. Puscher,[1] Meltem F. Aygüler,[2] Pablo Docampo,[2] Rubén D. Costa[1*]*

Bianka M. D. Puscher and Dr. Rubén D. Costa
Department of Chemistry and Pharmacy, University of Erlangen-Nuremberg (FAU),
Egerlandstr. 3, D-91058 Erlangen, Germany
E-mail: ruben.costa@fau.de
Meltem F. Aygüler and Dr. Pablo Docampo
Department of Chemistry and Center for Nanoscience, University of Munich (LMU),
Butenandtstr. 11, D-81377 Munich, Germany
E-mail: Pablo.docampo@cup.lmu.de

Keywords: perovskite nanoparticles, ionic-based devices, electrochemical impedance spectroscopy, light-emitting electrochemical cells

Hybrid and all-inorganic perovskite (PK) materials are a promising next generation of semiconducting materials due to their outstanding light-harvesting features that lead to high solar energy conversion efficiencies, as well as their color-tunable and efficient luminescent properties. Bulk PK films are both ionic and electronic conductors under the presence of an externally applied electric field. Herein, the internal ion motion behavior is demonstrated within PK nanoparticles in thin-film devices by means of different long-time poling schemes and both static and dynamic electrochemical impedance spectroscopy (EIS) assays. In particular, the existence of a dynamic device behavior is related to the migration and rearrangement of different ionic species upon applying different driving and poling schemes. The latter resembles the well-known signatures of the ionic motion in light-emitting electrochemical cells (LECs), that is, i) the formation of electrical double layers due to the ionic distribution at the electrodes' interfaces, ii) the growth of the doped regions once the charge injection is effective, and iii) the formation of a non-doped region in the bulk of the device. Hence, this comprehensive study

opens up an alternative route towards understanding the dynamics inside hybrid perovskite materials based on the large body of knowledge of LECs.

1. Introduction

Organic-inorganic halide perovskites (PK) have become the center of interest in photovoltaics since their breakthrough in 2012 as inexpensive, easily processable, and highly efficient light-harvesting materials. They consist of a three-dimensional $APbX_3$ structure (X = Cl, Br, and I), in which organic molecules (A) occupy the space between corner-sharing metal halide octahedra (PbX_6) forming a distorted Pm3m crystal structure.[1–3] Its organic-inorganic hybrid nature allows the preparation of thin films from solution based techniques at low temperatures, keeping the high degree of order and outstanding optoelectronic properties typical for inorganic materials.[2,4-8] This has led to an impressive solar energy conversion efficiency exceeding 22 %, as well as lighting devices with external quantum efficiencies up to 8.53 %.[1,9–24] Here, the emission color can be tuned by modifying the halide content and can span the whole visible and near infrared spectra.[7,14,25–27]

Despite the enormous advances in PK-based optoelectronics, both the intrinsic behavior of PK bulk films under electrical external stimuli and how it rules the devices mechanism is still under heavy debate.[28–32] In both photovoltaic and light-emitting devices additional capacitance features at the low frequency range under illumination are present,[28,33,34] while a poling effect is also present in the devices.[28] These effects are qualitatively postulated to be related to ion-migration under an applied electric field.[35–38] Here, theoretical calculations predict vacancy-assisted diffusion activation energies of 0.33-0.50 and 0.55-0.80 eV for positively charged halide vacancies and negatively charged methylammonium cation (MA^+) vacancies, respectively.[39–41] The corresponding model suggests that the halide migrates with a slightly curved pathway along the edges of the $PbBr_6$ octahedron, while the organic cation moves along the plane – **Scheme 1**.[40] The activation energy of the lead cation migration,

presumed along the diagonal of the unit cell – Scheme 1, was calculated to be much higher (~2.30 eV), resulting in a relatively immobile Pb^{2+} sublattice.[39,40] Indeed, while Eames *et al.* have already demonstrated the significant impact of I^- migration.[40,42] Wen *et al.* have recently found evidence in fluorescence imaging for both halide as well as MA^+ diffusion and accumulation at the interface when an external potential is applied.[43]

A model to study the ionic drift can be found in the simplest type of thin-film ionic-based lighting devices, that is, the light-emitting electrochemical cells (LECs). Recently, we have shown the first operating PK-based LEC devices using $MAPbBr_3$ and $FAPbBr_3$ nanoparticles (NP) directly blended with a standard ionic polyelectrolyte – *i.e.*, a star-like poly(ethylene oxide) derivative and $LiCF_3SO_3$.[12] Following up this contribution, Li *et al.* have demonstrated the dramatic impact of the inorganic salt on the device brightness and illustrated that devices with a blend of PK and a poly(ethylene oxide) exhibit both electronic and ionic conductivity.[15] On a different approach, Ling *et al.* and Li *et al.* have also realized efficient lighting devices by either blending PK nanoplatelets with a bipolar host material like (poly(9-vinylcarbazole):2-(4-biphenylyl)-5-phenyl-1,3,4-oxadiazole) (PVK:PBD) in combination with the electron transport layer bathocuproine (BCP) or blending nanocrystalline PKs with a polyimide precursor dielectric (PIP).[22,44] In parallel to these contributions, Zhang *et al.* investigated the dynamic behavior of perovskite bulk thin-film devices, stating a *modus operandi* that qualitatively resembles the one of LECs.[34] Taking all these findings into account, it seems to be safe to postulate that electrolyte-free PK NPs devices might feature an electrochemical response similar to a LEC device. This was briefly shown in our previous work,[12] in which the electrolyte-free devices show a moderate charge injection, without a luminance response.

To take this further, this work provides a more detailed understanding of the intrinsic dynamic behavior of ions in hybrid $MAPbBr_3$ perovskite nanoparticles (MPK NPs) applied in electrolyte-free thin-film devices with the same architecture to that of traditional LECs. This is

assessed by means of a joint analysis of the electrical device response over long periods of time under different poling schemes – *i.e.*, constant and pulsed driving modes – and electrochemical impedance spectroscopy (EIS) studies based on static and dynamic modes. We clearly demonstrate that in the long-term measurements, the electrochemical changes are defined by three different ionic distribution rearrangement time constants that are further corroborated by EIS assays. In addition, the latter allows us to compare the ion conductivity and dielectric constant of the MPK NPs in thin films, which are 1.37 x 10^{-6} S/m and 26.7, respectively. This is in agreement with those reported values measured in bulk thin film device, putting our results into the context of the current literature. Furthermore, all the results are compared to assays on all-inorganic $CsPbBr_3$ perovskite nanoparticles (CPK NPs) thin films using the same device structure. Overall, this work clearly demonstrates that the electrochemical behavior of PK NP based thin-film devices is the same as that of ionic-based devices.

2. Results and Discussion

2.1. Brief introduction to the mechanics of light-emitting electrochemical cells

The LECs consist of a single-layer architecture with an active layer based on a luminescent compound mixed with ionic additives that allow both electronic and ionic-assisted processes under operation conditions – **Figure 1** (left). In detail, the versatility of this technology is highlighted by the wide range of materials that can be applied, namely luminescent polymers, phosphorescent ionic transition metal complexes, luminescent nanoparticles and/or quantum dots, and small molecules.[12,45–61] The latter are blended with either ionic liquids or ionic polyelectrolytes that provide the necessary amount of mobile anions to assist the injection process upon applying a voltage over time.

Figure 1 (right) illustrates the LEC mechanism, that is, how the ions accumulate at both electrode interfaces, creating two thin layers of uncompensated ionic charges – *i.e.*, electric double layers (EDLs) – that facilitate the charge injection of electrons into the active layer.

Adjacent to the EDLs, the formation of highly conductive p- and n-type doped regions takes place, explaining the well-known slow turn-on time of these devices. The latter grow towards each other reducing the non-doped region width. This creates the so-called p-i-n junction, where the charge carriers recombine and emit light in the intrinsic region.[45,62-64] In this way, the potential between the EDLs are aligned as shown in the potential profile – Figure 1 (right).[45,65]

Although the LEC mechanism has been extensively studied in interdigitated device architectures, different groups have recently established how to study the LEC mechanism in sandwich-like devices by means of applying different driving schemes and electrochemical impedance spectroscopy (EIS).[45,49,62,66–69] As such, we have decided to apply these techniques to determine the behavior of PK NP electrolyte-free thin-film devices, and we were able to establish the resemblance of the PK device mechanism to the above mentioned LEC devices.

2.2. Preparation and characterization of PK NP devices

To provide a solid investigation, we compared two different PK NP materials: $MAPbBr_3$ (MPK) and $CsPbBr_3$ (CPK). Both NPs were prepared by following previous reports[7,12] and yielded colloidal dispersions with crystallite sizes of less than 10 nm for both compounds, although we observed bigger aggregates in MPK NPs. Transmission electron microscopy (TEM) images, X-ray diffraction (XRD), and emission spectra are given in the SI – **Figure S1, S2, and S3**. The thin films were prepared by spin-coating on top of indium tin oxide (ITO) substrates that were previously coated with a thin layer of poly(3,4-ethylenedioxythiophene) polystyrene sulfonate (PEDOT:PSS). The MPK NP and CPK NP films feature thicknesses of 100 and 50 nm, respectively – see Experimental Section for more details.

To ensure that the NPs do not undergo any degradation upon device fabrication, while thin and homogeneous films are guaranteed, the morphology and the photophysical features of both MPK NP and CPK NP films were investigated by both atomic force microscopy (AFM) and steady-state absorption and photoluminescence (PL) spectroscopy – **Figure 2** and **S4**. On one hand, AFM confirms a homogenous coverage with no particular aggregation or phase

separation features for both NP types, as well as a root-mean-square roughness of around 10-13 and 15-20 nm, respectively. On the other hand, the absoption and emission spectra of the films of MPK NPs show a narrow band at 525 nm and a near band edge of 530 nm with a full width at the half maximum (fwhm) of 38 nm. The features of CPK NPs are blue-shifted to an absorption band centered at 508 nm and an emission band located at 517 nm with a fwhm of 19 nm, indicating an increase of the optical band gap as a result of the Pb-Br-Pb angle variation caused by the cation exchange.[70,71] Overall, these features are in good agreement with bulk-like films and PK NP dispersions.[7,14,72]

To finalize the PK NP device, a 70 nm Aluminum cathode was evaporated onto the above-mentioned layers. The metal cathode was selected due to its work function that is much lower than the conduction band of perovskite, providing a lack of charge injection if the expected LEC *modus operandi* of PK NP devices is not present – Figure 1. Representative examples of luminance-current-voltage (LIV) characteristics are given in **Figure S5**. No detected EL was observed as in our previous results,[12] even if charge injection is present at 3.2 and 3.5 V for MPK and CPK NP devices, respectively.

2.3. Analysis of the mechanism of the PK NP devices

2.3.1. Studies based on applying different poling schemes

There are two possible poling schemes – *i.e.* constant external voltage and pulsed current – to study the response of the ions inside a film upon an electric potential. Since the ions feature different diffusion activation energies as stated in the introduction, differences in their motion rates, which are independent of the poling scheme, can be expected. **Figure 3** shows the time-dependent response of the current upon applying a constant external voltage. We noted an increase of the current density over a timeframe of 6 h (dotted line), which perfectly fits to a tri-exponential function. This is a typical feature of LECs and can be attributed to the slow

enhancement in charge injection processes due to the formation of the EDLs at the electrode interface and the subsequent growth of the doped regions.[45-47,49,63,67-69]

Here, we assign the shortest of the three processes to the fast formation of EDLs by halide drift (black ◀, τ_1 = 30 ± 1.5 sec) due to the lowest diffusion activation energy. This is in good agreement with other studies, where the effect of the diffusion of the halides was observed within a few seconds in photocurrent relaxation measurements and time-dependent PL imaging of $MAPbI_3$ perovskite bulk thin-film solar cells and layers – *i.e.*, ITO/c-TiO_2/$MAPbI_3$/*spiro*-OMeTAD/Au.[28,31,43] Since the activation energy does not differ drastically, the Br^- migration is likely in a similar time-scale. Given that MA^+ cations have higher diffusion activation energies than halides,[40] the second time constant (grey ▲, τ_2 = 12 ± 0.4 min) is presumably caused by either their alignment and migration towards the electrode interface. However, it could also be related to the differences in the energy level alignments between the perovskite's conduction/valence bands and the different electrodes – Figure 1, leading to short and long time constants to form effective EDLs at both the cathode and the anode. Regarding the accumulation of positive ions at an interface, Wen *et al.* found comparable results by studying time-resolved PL imaging.[43] The third and slowest process (dark grey ▼, τ_3 = 1.6 ± 0.1 h) is attributed to the growth of the charge carrier doped layers as it has been observed in LECs.[45,47,48,67-69] If there is a lack of device degradation, the current profile reaches a plateau at this point, at which it remains stable as shown by the dashed line – Figure 3. But, the MPK NP device clearly shows a linear decrease in current (light grey solid line) after 6 h (dotted line). This is typically related to over oxidation and/or reduction processes that degrade the thin films or the formation of pin-holes due to the film morphology that leads to an inhomogeneous distribution of the electric field strength.[73,74] In light of this result, we decided to apply a pulsed current driving scheme, which leads to fast redistribution processes that

significantly decelerate the degradation of the device, allowing the long-term studies of the device behavior.

In this case, the dynamic process of the ionic distribution rearrangement is observed by the voltage decay that is necessary to maintain the desired current flow. The benefits of this driving scheme are clearly seen in the excellent stability of the applied voltage over a timeframe of a day – **Figure 4** (left). In a similar way to the results obtained for devices driven at constant voltage, the average voltage decay over time also follows a tri-exponential decay function – Figure S4 (right). Furthermore, we have studied the changes in the kinetics at different applied currents – Figure 4 (left) and **Table 1**. Despite increased current density that causes a stronger electric field, we do not observe a significant shortening of the τ_3 values. We explain this by the extending EDLs that screen the electric field generated at the electrode interface[45,47,48,67-69] – Figure 1 (right). Hence, the growth of the doped regions might be solely ruled by the intrinsic electronic conductivity of the material.[75,76] The decay times τ_1 and τ_2 show similar values for all the applied pulsed currents, since the resulting voltage is excessively exceeding the required activation energy for the ion migration. In this regard, it is important to point out the difference between τ_1 and τ_2 in MPK and CPK devices. The latter shows shorter τ_1 and larger τ_2 than MPK devices – Table 1. This can be explained by the energy level misalignment between the materials and the electrodes: 0.8 *vs.* 1.4 eV at the anode and 1.0 *vs.* 0.5 eV at the cathode for MPK and CPK devices, respectively – Figure 1 (left).

Another way to attest the motion behavior of the PK NP thin-film devices is to study the memory effect caused by the back motion of the ions into the bulk when the externally applied electrical potential is switched off. In this context, a set of devices were driven at a pulsed current of 50 mA for a short time of 8 min, followed by a switch off time of either 10 min or 3.5 h before the measurement was restarted at a pulsed current of 50 mA – Figure 4 (right) and **Table 2**. Taking into account the values of τ_1 and τ_2 as shown in Table 1, a time

frame of 8 min was chosen to ensure sufficient ion diffusion to study the EDL formation without causing pronounced electrochemical doping and thus conductivity changes. Indeed, the decay of the average voltage of the pulsed scheme of a fresh device obeys a bi-exponentially decay function – Figure 4 (right) in black squares, giving a τ_1 of 15.5 ± 2.5 sec and a τ_2 of 2.9 ± 0.3 min. After a switch-off time of 10 min (light grey diamonds) the desired current of 50 mA is already reached at an initial average voltage of 2.2 V, which is a 0.51 V lower voltage response than the one needed for the pristine device. In addition, the decay was found to be mono-exponential (τ_2 = 2 ± 0.2 min). Importantly, the short formation time of the EDLs caused by the halides was not observable, which is in agreement with the EDL-induced lower initial applied voltage compared to the fresh device. This indicates that the initial random ion distribution is not fully recovered. Next, a long switch-off time of around 3.5 h was studied. Driving the device afterwards at a pulsed current of 50 mA (grey circles) results in an increased initial average voltage (2.5 V). The bi-exponential behavior matches the one of the pristine device with τ_1 of 10.0 ± 1.0 sec and τ_2 of 3.0 ± 0.2 min. In both cases the average voltage at the end (τ = 4 – 8 min) decreases further than in the first measurement, which we attributed to either i) a polarization memory effect of the layer or ii) to a progressing doped layer formation.[28,37,40,42] In any case, these results strongly suggest a memory effect in the PK NP based device related to the slow back ion diffusion into the crystal lattice distribution similar to the PK NP fresh device.

Finally, CPK NP-based devices were studied in the same manner in order to support our hypothesis – **Figure S5**.[7,14] Here, the decrease of the average voltage exhibits a bi-exponential function, featuring a shorter τ_1 (8 ± 2 sec) and longer τ_2 (10 ± 2 min) values – Table 2. Since it is, in general, considered that all-inorganic PKs feature higher electronic conductivities than the hybrid ones,[77] shorter τ_3 times are expected for CPK NPs. After a period of 30 min, however, the average voltage response increases, revealing a shortened lifetime and, thus,

reduced stability of CPK NP films upon injection; this renders it impossible to study the formation of doped layers (τ_3). The reversibility of the CPK devices is also reflected in both τ_1 (11 ± 0.7 sec) and τ_2 (4.9 ± 0.5 min) – Figure S5 (right) and Table 2. In detail, after a switch-off time of 10 min, τ_1 was found to be the same as in the pristine device (11 ± 1.0 sec), indicating a strong memory effect related to the ion vacancy restoration. τ_2 is strongly reduced to 1.8 ± 0.1 min due to the smaller energy gap at the cathode side – *vide supra*. In a similar way to that noted for MPK NP devices, a switch-off time of 3.5 h leads to an initial applied voltage that is only 0.13 V lower than that of the fresh device.

Overall, our results indicate that PK NP based devices follow the same *modus operandi* as LECs. The evaluation of the electrical device behavior under applied different voltages shows that three different processes are present in the PK-devices. The shortest ones with an average time constant of 10-20 sec and 5-10 min are related to the formation of the EDLs at different electrode sides, which seems to be ruled by the different energy gap between the bulk film at the electrodes as the direct comparison between MPK and CPK devices suggested – Tables 1 and 2. Both lead to the formation of EDLs (τ_1 and τ_2) that facilitate the charge injection and subsequent growth of the doped regions (τ_3).

2.3.2. Analysis based on electrochemical impedance spectroscopy

Having demonstrated that electrolyte-free PK NP devices show a LEC *modus operandi*, we decided to further investigate this unique dynamic behavior by means of EIS investigations. This technique has emerged as a powerful tool, since electronic and ionic charge carriers of mixed conductors are easily distinguished by the probed frequency.[67,69] Furthermore, this technique allows two type of experiments, namely: (i) static, by performing EIS assays at different voltages; and (ii) dynamic, by applying a constant voltage and periodically performing

EIS analysis over the driving time. The parameters gained by these measurements are composed of a real part and an imaginary part according to:

$$\frac{1}{Z} = \frac{i_{ac}}{v_{ac}} = |\Delta Z| e^{i\varphi} = G(\omega) + i\omega C(\omega) \quad (1)$$

where ω, Z, G, and C represent the angular frequency, the impedance, the conductance, and the capacitance of the system, respectively.

To provide reliable fittings, the capacitance was replaced with a constant phase element (CPE) due to non-uniform current density distribution and/or reaction rates along the electrode surface, usually caused by an inhomogeneous surface.[68,78] A more detailed explanation of the measurement is provided in the SI. The circuit models used for LECs was suggested by Munar *et al.*[67] and already applied for PK-based LECs by Zhang *et al.*[34] The model is given in **Figure 5** (left), with R_i for the resistance of the ion diffusion that is visible at the low frequency regime and CPE_{EDL} as the capacitance caused by the redistribution of ions at the electrodes – *i.e.*, this circuit is related to the EDL formation.[69] R_e and C_g correspond to the electrical resistance and the geometrical capacitance of the active layer, respectively. The inductor corresponds to the inductance caused by the cables and was found to be 1.2±0.6 µH for all devices.[34,67,79]

Based on the time constants obtained from our pulsed current results (10 sec and longer), frequencies at a maximum of 0.1 Hz or preferably lower are needed to directly observe the drift of halide vacancies. Unfortunately, our EIS setup cannot reliably measure frequencies lower than 50 Hz for PK NP devices due to the low current flow and/or poor signal/noise ratio caused by the low electrical conductivity of the films. However, the fitting allows a consistent estimation of the resistance associated to the EDLs when the dynamic EIS assays are performed as the device is driven for a long period of time and undergoes less stark changes than it does for the static mode during which the external applied potential increases every two minutes. In contrast, the static EIS measurements are too fast to allow a meaningful response of the formation of the EDLs, causing a disturbance in the low frequency range – **Figure S7**. As such,

a simple electrical circuit based on R_e and C_{geo} was chosen for the static assays – Figure 5 (right). All Nyquist plots are provided in the SI.

Static electrochemical impedance spectroscopy assays

The static EIS of both MPK and CPK NP devices were measured at different voltages from 0 V to 4.5 V in 0.5 V steps, while each measurement takes about 2 min. **Figure 6** and **S8** show the R_e plotted against the applied bias, revealing two different slope behaviors, namely one below – *i.e.*, 0-2.5 V – and one above – *i.e.*, 2.5-4.5 V – the PK NP materials' band gap (2.5 eV). The earlier shows a mono-exponential slope that resembles the unique feature of LECs with respect to the EDL formation that ultimately lowers the injection resistance. In detail, it reduces until 1.5 V and reaches a plateau up to 2.5 V. In CPK NP devices (Figure S8), the movement does not attain a final state, as the resistance change never reaches a stable value. At applied voltages beyond the band gap of the material, a linear slope is related to an effective charge injection process that causes the growth of the doped layer. As a result, the electrical resistance in the non-doped region of the film is further reduced, as this region is getting thinner. To the best of our knowledge, we note that this two-slope-behavior, which is typical for LECs, has not been observed in PK films.[67-69] This, indeed, corroborates the results obtained upon inspection of the electrical behavior of the devices under different poling conditions – Section 2.3.1.

For both PK NP devices, the resistance changed by one order of magnitude until the band gap was reached. Due to the lower activation energy of the halide diffusion, the overall resistance is lower for CPK NP. Yet, going from 0 V to 2 V, the resistance R_e in MPK NP reduced more than twice compared to the trend noted for CPK NP films. This implies that the ionic distribution rearrangement inside CPK NP films has a much smaller effect than in MPK NP films.

To provide a full understanding, the frequency-dependent resistance, phase angle, conductance, and capacitance results were analyzed – **Figure 7** and **S9**. At an applied voltage

of 1.5 V, where no injection took place yet, the growth of EDLs is the dominant process. Although the diffusion of the halide is too fast to be monitored by the static assays, there is still a dynamic and ongoing process observable. As shown in Figure 6, the R_e is reduced and the conductance increases until 1.5 V. This corresponds to the resistance and conductance plateau at $f \leq 1000$ Hz – Figure 7. Additionally, the phase angle maximum is lower and shifts to higher frequencies. This is known to be a direct observation of growing EDLs from the electrodes.[67-69]

In CPK NP devices the growth of EDLs is also present – Figure S9. At 4 V, the MPK NP device features only slight changes of the resistance and the conductance that is associated to a shift to high frequencies and a small lowering of the phase angle. This reflects the on-going but slow resizing of the non-doped layer for MPK NP in contrast to the significant resistance and conductance change for CPK NP device, indicating a higher conductivity of CPK NP.

To corroborate this notion, the 0 V EIS measurement is of special interest, as the layer is not altered in any way yet – Figure 7, black squares. Therefore, the materials' characteristic – *i.e.*, the dielectric constant (ε_r) and the ionic conductivity (σ) – can be obtained with equations 2 and 3.

$$\sigma = \frac{GL}{A} \tag{2}$$

$$C = \frac{\varepsilon_0 \varepsilon_r A}{L} \tag{3}$$

where L = 100 nm is the thickness of the active layer, A = 15 mm² the active area of the device, C is the effective capacitance, and ε_0 the vacuum permittivity (8.85 x 10^{-12} F/m).

Here, at 0 V high ion conductivities of 1.37 x 10^{-6} and 1.42 x 10^{-6} S/m and dielectric constants of 26.7 and 26.3 were calculated for MPK and CPK NP devices, respectively. Reference data was found in the literature for only two of these values. On one hand, a close value for the dielectric constant of around 25.5 was reported for $MAPbBr_3$ crystals.[80] On the other hand, temperature dependent ion conductivity measurements of $CsPbBr_3$ were already

reported in the 80s, indicating values from 3.30 x 10^{-6} to 1.38 x 10^{-5} S/m at temperatures from 30 °C to 90 °C.[81] Both values are in line to those values obtained from the static EIS analysis. Indeed, even if a direct comparison with the literature is not possible, an ion conductivity with approximate values between 10^{-6} and 10^{-7} S/m was found for $MAPbI_3$ thin films.[34]

Dynamic electrochemical impedance spectroscopy assays

As the last step in our investigation, we performed dynamic EIS measurements to observe the slow ionic distribution rearrangement and the growth of the doped region over time at applied constant voltage of 3 V. Here, EIS assays were performed every half an hour over a total time period of 12 h, allowing the fitting with the full electric circuit, in which the R_i of the EDLs is considered – Figure 5 (left). The corresponding conductance and capacitance at 0.5, 2, 4, 8, and 12 h as well as the-figures-of-merit as a function of time are shown in **Figure 8**. The experiment was not possible with CPK NP devices due to their intrinsic instability – Figure S6.

Comparable with the results derived from the pulsed mode analysis, the internal ion movement of the MPK NP devices is attested by the decrease of the resistance over time. Reflecting the on-going EDL growth, the R_i decreases over time, showing a mono-exponential decay with a time constant of $\tau_i = 4.1 \pm 1.3$ h. During this timeframe, the C_{eff} slightly increases, suggesting a small charge injection process. This holds true until 4 h at which time the C_{eff} starts to dramatically increase as the doped regions grow towards each other and thus reduce the less conductive, intrinsic zone even more. Finally, this is likely the reason for the degradation of the PK NPs as shown in Figure 3. The long timeframe of 4 h cannot be attributed to the halide and cation diffusion alone, indicating that the regions are not strictly differentiated. The R_e reduces greatly and slowly converges to the values of R_i. Given the formation of the doped layers in the bulk, the R_e decay should correlate with τ_3 determined by the pulsed mode measurements. In fact, the mono-exponential decay of R_e results in a time constant of $\tau_e = 1.3 \pm 0.1$ h, which is in agreement with those summarized in Table 1.

3. Conclusion

In this work, we have demonstrated that pristine hybrid $MAPbBr_3$ and all-inorganic $CsPbBr_3$ NP thin-film devices behave in a similar way to ionic-based lighting devices such as LECs. This is supported by a comprehensive study including different long-time poling schemes and both static and dynamic EIS assays. Here, our results show that the current and voltage response obey a tri-exponential function similar to what would be expected in LECs. In this way, we attributed the two short processes to the formation of the EDLs at different electrode interfaces and the long process to the gradual formation of the doped regions. The nature of these processes was also corroborated by determining a memory effect. Through static and dynamic EIS analysis, we also confirmed the effect of the internal ion movement on the device behavior. In detail, we observe the formation of EDLs under applied voltages lower than the band gap of the NPs, as well as the growth of the doped region over time. We note that EIS analysis also allowed us to determine the ionic conductivity and the dielectric constant feature of PK NP based films. The latter were found to be in excellent agreement with the values reported in the literature. Overall, this work asserts that the ionic dynamic processes are valid for probably all type of PK NP – like $FAPbBr_3$, $MAPbI_3$, and all type of mixed perovskite materials – based devices, which might have a similar mechanism description as those observed in LECs. In this rational line, we propose that enhancing the ionic interlayers by blending the material with already known electrolytes can result in enhanced efficiency and stability feature in both photovoltaic and lighting technologies.

4. Experimental Section

All materials were purchased from Sigma Aldrich and used as received if it is not stated differently.

Synthesis: MPK NPs were synthesized by slightly changing the reported literature.[12,82] MPK NPs were prepared by consecutively dissolving octylammonium bromide and lead

bromide in a warm solution (80°C) of oleic acid (OA) in octadecene (ODE). In the next step, methylammonium bromide was added dropwise and finally tetrahydrofuran was used as a precipitating agent. For the CPK NPs, ODE and $PbBr_2$ were dried under vacuum for 1 h at 120°C. Dried oleylamine (Acros Organics) and dried OA were injected to the flask at 120°C under N_2 atmosphere. After all $PbBr_2$ was solubilized, the temperature was increased to 170°C and Cs-oleate solution (prepared by the reaction of OA and Cs_2CO_3 in ODE) was quickly injected. The reaction mixture was cooled by ice-water bath, subsequently centrifuged at 10000 rpm for 10 min and redispersed in hexane.[7]

Device Preparation: ITO coated glass (Naranjo Substrates) were cleaned *via* sequential ultrasonic baths in detergent, water, acetone, and 2-propanol solvents for 15 min respectively. Subsequently the substrates were dried and treated in an UV–ozone cleaner (Jelight 42-220) for 10 min. A PEDOT:PSS (Clevios P VPAI 4083) layer was doctor-bladed (400 µm substrate distance and 10 mm/s speed) onto the ITO-glass substrate and annealed at 120 °C for 20 min. Both types of PK NPs were spin-coated at 400 rpm for 3 min for MPK NPs and at 1000 rpm for 30 sec for CPK NPs as high concentrated, yellow suspension (2 mg/ml in chlorobenzene and 10 mg/ml in hexane for MPK and CPK NPs, respectively) on top of either quartz slides or the PEDOT:PSS layer. Independent of the type of substrate, the MPK NP and CPK NP films feature thicknesses of 100 and 50 nm, respectively, as determined by alpha-step profilometry. Afterward they were transferred into an inert atmosphere (<0.1 ppm O_2 and H_2O, Innovative Technology) where it was dried at 60 °C for 10 min. Finally an aluminum cathode electrode (90 nm) was applied with a shadow mask and thermal evaporation (Angstrom Covap) under high vacuum ($<1\times10^{-6}$ mbar). All measurements were performed in inert atmosphere and in the dark.

Measurement techniques and equipment: TEM measurements were performed with a JEM-2011 (JEOL) equipped with LaB6 operated at 200 kV and an EDS (EDAX) detector. The layer thickness was determined using a Bruker 'DektakxT' profilometer. AFM characterization

was carried out under ambient conditions using SPM Nanoscope Illa multimode working in tapped mode with a HQ:NSC15/AL BS tip (μMasch) at a working frequency of ~325 kHz. The powder XRD measurements were performed on a Huber Imaging Plate Guinier Diffractiometer G670 (Cu Kα1 radiation). Steady-state absorption and emission features were performed with a Perkin Elmer LS50 spectrofluorometer and a SPECORD® S 600. Current-Voltage-sweeps (IVs), as well as time dependent current and voltage measurements by applying constant voltage and pulsed current were performed in a Botest OLT OLED Lifetime-Test System. For the IV assay shown in Figure S5 a ramp from 0 to 10 V using 0.25 V steps was applied. Although AFM morphology studies (Figure S4) indicate that the PK NP films are homogenous, the electrical behavior of the devices often shows that small pin-holes caused by film defects cannot be avoided. By running one LIV, the pin-holes self-repair providing reproducible results independent on the applied technique.[83] Hence, a IV sweep (0-10 V, with 0.5 V steps) was performed to all the devices before further analysis. The pulsed current driving scheme was performed by using 500 µs intervals of an applied current – *e.g.*, 7, 20, 50, and 80 mA. The voltage response of both intervals is then recorded and the average voltage of both plotted against time. The EIS assays were carried out with a potentiostat (Metrohm µAutolabIII) equipped with a frequency response analyzer module (FRA2). The devices were measured in the frequency range from 500 kHz to 50 Hz and with an amplitude of 10 mV. Its data was evaluated using the software NOVA 1.11; the stability of the NPs in this experiment was evaluated by Kronig-Kramers transformation – Figure S12. More information about this is given in the Supplementary Information.

Supporting Information

Supporting Information is available from the Wiley Online Library or from the author.

Acknowledgements

The authors acknowledge funding from the German Federal Ministry of Education and Research (BMBF) under the agreement number 01162525/1, the Bavarian Ministry of the Environment and Consumer Protection, and the "Engineering of Advanced Materials" (EAM) as well as the DFG Excellence Cluster Nanosystems Initiative Munich (NIM). R.D.C. acknowledges the Fonds der Chemischen Industrie (FCI) in the Liebig grant framework. R.D.C. thanks Prof. Dirk M. Guldi for his kind support and advices. P. D. acknowledges support from the European Union through the award of a Marie Curie Intra-European Fellowship.

Received: ((will be filled in by the editorial staff))
Revised: ((will be filled in by the editorial staff))
Published online: ((will be filled in by the editorial staff))

References

[1] Y.-H. Kim, H. Cho, J. H. Heo, T.-S. Kim, N. Myoung, C.-L. Lee, S. H. Im, T.-W. Lee, *Adv. Mater.* **2015**, *27*, 1248.
[2] N.-G. Park, *Mater. Today* **2015**, *18*, 65.
[3] S. Kazim, M. K. Nazeeruddin, M. Graetzel, S. Ahmad, *Angew. Chem. Int. Ed.* **2014**, *53*, 2812.
[4] Y. Chen, J. Peng, D. Su, X. Chen, Z. Liang, *ACS Appl. Mater. Interfaces* **2015**, *7*, 4471.
[5] H.-S. Kim, C.-R. Lee, J.-H. Im, K.-B. Lee, T. Moehl, A. Marchioro, S.-J. Moon, R. Humphry-Baker, J.-H. Yum, J. E. Moser, M. Grätzel, N.-G. Park, *Sci. Rep.* **2012**, *2*, 591.
[6] S. D. Stranks, G. E. Eperon, G. Grancini, C. Menelaou, M. J. P. Alcocer, T. Leijtens, L. M. Herz, A. Petrozza, H. J. Snaith, *Science* **2013**, *342*, 341.
[7] L. Protesescu, S. Yakunin, M. I. Bodnarchuk, F. Krieg, R. Caputo, C. H. Hendon, R. X. Yang, A. Walsh, M. V. Kovalenko, *Nano Lett.* **2015**, *15*, 3692.
[8] X. Zhang, H. Lin, H. Huang, C. Reckmeier, Y. Zhang, W. C. H. Choy, A. L. Rogach, *Nano Lett.* **2016**, *16*, 1415.
[9] N. J. Jeon, J. H. Noh, W. S. Yang, Y. C. Kim, S. Ryu, J. Seo, S. Il Seok, *Nature* **2015**, *517*, 476.
[10] H. P. Zhou, Q. Chen, G. Li, S. Luo, T. B. Song, H. S. Duan, Z. R. Hong, J. B. You, Y. S. Liu, Y. Yang, *Science* **2014**, *345*, 542.
[11] P. Docampo, J. M. Ball, M. Darwich, G. E. Eperon, H. J. Snaith, *Nat. Commun.* **2013**, *4*, 1.
[12] M. F. Aygüler, M. D. Weber, B. M. D. Puscher, D. D. Medina, P. Docampo, R. D. Costa, *J. Phys. Chem. C* **2015**, *119*, 12047.
[13] N. K. Kumawat, A. Dey, K. L. Narasimhan, D. Kabra, *ACS Photonics* **2015**, *2*, 349.
[14] J. Song, J. Li, X. Li, L. Xu, Y. Dong, H. Zeng, *Adv. Mater.* **2015**, *27*, 7162.
[15] J. Li, S. G. R. Bade, X. Shan, Z. Yu, *Adv. Mater.* **2015**, *27*, 5196.
[16] H. Cho, S.-H. Jeong, M.-H. Park, Y.-H. Kim, C. Wolf, C.-L. Lee, J. H. Heo, A. Sadhanala, N. Myoung, S. Yoo, S. H. Im, R. H. Friend, T.-W. Lee, *Science* **2015**, *350*, 1222.
[17] N. Ahn, D. Y. Son, I. H. Jang, S. M. Kang, M. Choi, N. G. Park, *J. Am. Chem. Soc.* **2015**, *137*, 8696.

[18] W. Nie, H. Tsai, R. Asadpour, J.-C. Blancon, A. J. Neukirch, G. Gupta, J. J. Crochet, M. Chhowalla, S. Tretiak, M. A. Alam, H.-L. Wang, A. D. Mohite, *Science* **2015**, *347*, 522.
[19] F. Giordano, A. Abate, J. Pablo, C. Baena, M. Saliba, T. Matsui, S. H. Im, S. M. Zakeeruddin, M. K. Nazeeruddin, A. Hagfeldt, M. Graetzel, *Nat. Commun.* **2016**, *7*, 1.
[20] S. G. R. Bade, J. Li, X. Shan, Y. Ling, Y. Tian, T. Dilbeck, T. Besara, T. Geske, H. Gao, B. Ma, K. Hanson, T. Siegrist, C. Xu, Z. Yu, *ACS Nano* **2016**, *10*, 1795.
[21] J. Wang, N. Wang, Y. Jin, J. Si, Z. K. Tan, H. Du, L. Cheng, X. Dai, S. Bai, H. He, Z. Ye, M. L. Lai, R. H. Friend, W. Huang, *Adv. Mater.* **2015**, *27*, 2311.
[22] Y. Ling, Z. Yuan, Y. Tian, X. Wang, J. C. Wang, Y. Xin, K. Hanson, B. Ma, H. Gao, *Adv. Mater.* **2016**, *28*, 305.
[23] S. I. S. Woon Seok Yang, Jun Hong Noh, Nam Joong Jeon, Young Chan Kim, Seungchan Ryu, Jangwon Seo, *Science* **2015**, *348*, 1234.
[24] M. Saliba, T. Matsui, J.-Y. Seo, K. Domanski, J.-P. Correa-Baena, N. Mohammad, S. M. Zakeeruddin, W. Tress, A. Abate, A. Hagfeldt, M. Gratzel, *Energy Environ. Sci.* **2016**, *9*, 1989.
[25] F. Zhang, H. Zhong, C. Chen, X. Wu, X. Hu, H. Huang, *ACS Nano* **2015**, *3*, 4533.
[26] G. Xing, N. Mathews, S. S. Lim, N. Yantara, X. Liu, D. Sabba, M. Grätzel, S. Mhaisalkar, T. C. Sum, *Nat. Mater.* **2014**, *13*, 476.
[27] O. A. Jaramillo-Quintero, R. S. Sánchez, M. Rincón, I. Mora-Sero, *J. Phys. Chem. Lett.* **2015**, *6*, 1883.
[28] Z. Xiao, Y. Yuan, Y. Shao, Q. Wang, Q. Dong, C. Bi, P. Sharma, A. Gruverman, J. Huang, *Nat. Mater.* **2015**, *14*, 193.
[29] H. J. Snaith, A. Abate, J. M. Ball, G. E. Eperon, T. Leijtens, N. K. Noel, S. D. Stranks, J. T. W. Wang, K. Wojciechowski, W. Zhang, *J. Phys. Chem. Lett.* **2014**, *5*, 1511.
[30] J. A. Christians, J. S. Manser, P. V. Kamat, *J. Phys. Chem. Lett.* **2015**, *6*, 852.
[31] E. L. Unger, E. T. Hoke, C. D. Bailie, W. H. Nguyen, A. R. Bowring, T. Heumuller, M. G. Christoforo, M. D. McGehee, *Energy Environ. Sci.* **2014**, *7*, 3690.
[32] A. R. Pascoe, N. W. Duffy, A. D. Scully, F. Huang, Y.-B. Cheng, *J. Phys. Chem. C* **2015**, *119*, 4444.
[33] H. Kim, I. Mora-Sero, V. Gonzalez-Pedro, F. Fabregat-Santiago, E. J. Juarez-Perez, N. Park, J. Bisquert, *Nat. Commun.* **2013**, *4*, 2242.
[34] H. Zhang, H. Lin, C. Liang, H. Liu, J. Liang, Y. Zhao, W. Zhang, M. Sun, W. Xiao, H. Li, S. Polizzi, D. Li, F. Zhang, Z. He, W. C. H. Choy, *Adv. Funct. Mater.* **2015**, *25*, 7226.
[35] J. Mizusaki, K. Arai, K. Fueki, *Solid State Ionics* **1983**, *11*, 203.
[36] T. A. Kuku, *Thin Solid Films* **1998**, *325*, 246.
[37] Y. Yuan, J. Huang, *Acc. Chem. Res.* **2016**, *49*, 286.
[38] G. Richardson, S. E. J. O'Kane, R. G. Niemann, T. A. Peltola, J. M. Foster, P. J. Cameron, A. B. Walker, *Energy Environ. Sci.* **2016**, *9*, 1476.
[39] A. Walsh, D. O. Scanlon, S. Chen, X. G. Gong, S.-H. Wei, *Angew. Chem. Int. Ed.* **2015**, *54*, 1791.
[40] C. Eames, J. M. Frost, P. R. F. Barnes, B. C. O'Regan, A. Walsh, M. S. Islam, *Nat. Commun.* **2015**, *6*, 7497.
[41] J. Haruyama, K. Sodeyama, L. Han, Y. Tateyama, *J. Am. Chem. Soc.* **2015**, *137*, 10048.
[42] A. M. A. Leguy, J. M. Frost, A. P. McMahon, V. G. Sakai, W. Kochelmann, C. Law, X. Li, F. Foglia, A. Walsh, B. C. O'Regan, J. Nelson, J. T. Cabral, P. R. F. Barnes, *Nat. Commun.* **2015**, *6*, 7124.
[43] X. Wen, S. Huang, S. Chen, X. Deng, F. Huang, Y. Cheng, M. Green, A. Ho-Baillie, *Adv. Mater. Interfaces* **2016**, *3*, 1600467.
[44] G. Li, Z. K. Tan, D. Di, M. L. Lai, L. Jiang, J. H. W. Lim, R. H. Friend, N. C. Greenham, *Nano Lett.* **2015**, *15*, 2640.
[45] R. D. Costa, E. Ortí, H. J. Bolink, F. Monti, G. Accorsi, N. Armaroli, *Angew. Chem. Int.*

Ed. **2012**, *51*, 8178.
[46] M. D. Weber, M. Adam, R. R. Tykwinski, R. D. Costa, *Adv. Funct. Mater.* **2015**, *25*, 5066.
[47] H.-C. Su, J.-H. Hsu, *Dalt. Trans.* **2015**, *44*, 8330.
[48] A. Pertegás, D. Tordera, J. J. Serrano-Pérez, E. Ortí, H. J. Bolink, *J. Am. Chem. Soc.* **2013**, *135*, 18008.
[49] S. B. Meier, D. Tordera, A. Pertegás, C. Roldán-Carmona, E. Ortí, H. J. Bolink, *Mater. Today* **2014**, *17*, 217.
[50] M. S. Subeesh, K. Shanmugasundaram, C. D. Sunesh, T. P. Nguyen, Y. Choe, *J. Phys. Chem. C* **2015**, *119*, 23676.
[51] A. J. Norell Bader, A. A. Ilkevich, I. V. Kosilkin, J. M. Leger, *Nano Lett.* **2011**, *11*, 461.
[52] H.-C. Su, C.-Y. Cheng, *Isr. J. Chem.* **2014**, *54*, 855.
[53] G. Qian, Y. Lin, G. Wantz, A. R. Davis, K. R. Carter, J. J. Watkins, *Adv. Funct. Mater.* **2014**, *24*, 4484.
[54] S. Tang, W. Y. Tan, X. H. Zhu, L. Edman, *Chem. Commun.* **2013**, *49*, 4926.
[55] T. Hu, L. He, L. Duan, Y. Qiu, *J. Mater. Chem.* **2012**, *22*, 4206.
[56] K. Shanmugasundaram, M. S. Subeesh, C. D. Sunesh, R. K. Chitumalla, J. Jang, Y. Choe, *Org. Electron.* **2015**, *24*, 297.
[57] A. Sandström, L. Edman, *Energy Technol.* **2015**, *3*, 329.
[58] M. S. Subeesh, K. Shanmugasundaram, C. D. Sunesh, Y. S. Won, Y. Choe, *J. Mater. Chem. C* **2015**, *3*, 4683.
[59] K. T. Weber, K. Karikis, M. D. Weber, P. B. Coto, A. Charisiadis, D. Charitaki, G. Charalambidis, P. Angaridis, A. G. Coutsolelos, R. D. Costa, *Dalt. Trans.* **2016**, *45*, 13284.
[60] M. D. Weber, V. Nikolaou, J. E. Wittmann, A. Nikolaou, P. A. Angaridis, G. Charalambidis, C. Stangel, A. Kahnt, A. G. Coutsolelos, R. D. Costa, *Chem. Commun.* **2016**, *52*, 1602.
[61] M. D. Weber, J. E. Wittmann, A. Burger, O. B. Malcıoğlu, J. Segarra-Martí, A. Hirsch, P. B. Coto, M. Bockstedte, R. D. Costa, *Adv. Funct. Mater.* **2016**, *26*, 6737.
[62] S. Tang, L. Edman, *Top. Curr. Chem.* **2016**, *374*:40.
[63] N. Jürgensen, J. Zimmermann, A. J. Morfa, G. Hernandez-sosa, *Nat. Publ. Gr.* **2016**, 4.
[64] K. Lin, L. D. Bastatas, K. J. Suhr, M. D. Moore, B. J. Holliday, M. Minary-Jolandan, J. D. Slinker, *ACS Appl. Mater. Interfaces* **2016**, DOI 10.1021/acsami.6b03458.
[65] T. J. Mills, M. C. Lonergan, *Phys. Rev. B - Condens. Matter Mater. Phys.* **2012**, *85*, 1.
[66] D. Tordera, S. Meier, M. Lenes, R. D. Costa, E. Ortí, W. Sarfert, H. J. Bolink, *Adv. Mater.* **2012**, *24*, 897.
[67] A. Munar, A. Sandström, S. Tang, L. Edman, *Adv. Funct. Mater.* **2012**, *22*, 1511.
[68] S. B. Meier, D. Hartmann, A. Winnacker, W. Sarfert, *J. Appl. Phys.* **2014**, *116*, 104504.
[69] S. van Reenen, R. A. J. Janssen, M. Kemerink, *Adv. Funct. Mater.* **2012**, *22*, 4547.
[70] Y. Rakita, S. R. Cohen, N. K. Kedem, G. Hodes, D. Cahen, *Arxiv Prepr.* **2015**, *3*, 1.
[71] M. Mittal, A. Jana, S. Sarkar, P. Mahadevan, S. Sapra, *J. Phys. Chem. Lett.* **2016**, *7*, 3270.
[72] F. C. Hanusch, E. Wiesenmayer, E. Mankel, A. Binek, P. Angloher, C. Fraunhofer, N. Giesbrecht, J. M. Feckl, W. Jaegermann, D. Johrendt, T. Bein, P. Docampo, *J. Phys. Chem. Lett.* **2014**, *5*, 2791.
[73] F. Altal, J. Gao, *Org. Electron.* **2015**, *18*, 1.
[74] S. B. Meier, D. Hartmann, D. Tordera, H. J. Bolink, A. Winnacker, W. Sarfert, *Phys. Chem. Chem. Phys.* **2012**, *14*, 10886.
[75] Q. Pei, Yang, G. Yu, C. Zhang, A. J. Heeger, *J. Am. Chem. Soc.* **1996**, *118*, 3922.
[76] J. A. Manzanares, H. Reiss, A. J. Heeger, *J. Phys. Chem. B* **1998**, *102*, 4327.
[77] D. W. Lynch, *Phys. Rev.* **1960**, *118*, 468.
[78] G. J. Brug, A. L. G. van den Eeden, M. Sluyters-Rehbach, J. H. Sluyters, *J. Electroanal.*

Chem. Interfacial Electrochem. **1984**, *176*, 275.
[79] L. D. Bastatas, K. Lin, M. D. Moore, K. J. Suhr, M. H. Bowler, Y. Shen, B. J. Holliday, J. D. Slinker, *Langmuir* **2016**, DOI 10.1021/acs.langmuir.6b02415.
[72] M. I. Saidaminov, A. L. Abdelhady, B. Murali, E. Alarousu, V. M. Burlakov, W. Peng, I. Dursun, L. Wang, Y. He, G. Maculan, A. Goriely, T. Wu, O. F. Mohammed, O. M. Bakr, *Nat. Commun.* **2015**, *6*, 7586.
[73] M. V. S. Narayan, R. Lakshmisarma, S. V. Suryanarayana, *J. Mater. Sci. Lett.* **1987**, *6*, 93.
[74] L. C. Schmidt, A. Pertegás, S. González-Carrero, O. Malinkiewicz, S. Agouram, G. Mínguez Espallargas, H. J. Bolink, R. E. Galian, J. Pérez-Prieto, *J. Am. Chem. Soc.* **2014**, *136*, 850.
[75] D. Xu, Z. Deng, J. Xiao, D. Guo, J. Hao, Y. Zhang, Y. Gao, C. Liang, *J. Lumin.* **2007**, *122*, 642.

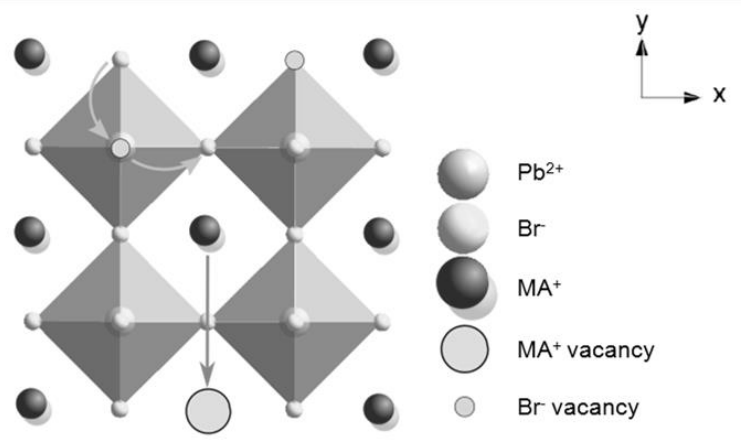

Scheme 1. Illustration of the perovskite crystal structure with migration paths of the halides along the edges of the $PbBr_6^{4-}$ octahedron (light grey) and of the organic cations in the MA-Br plane (dark grey).

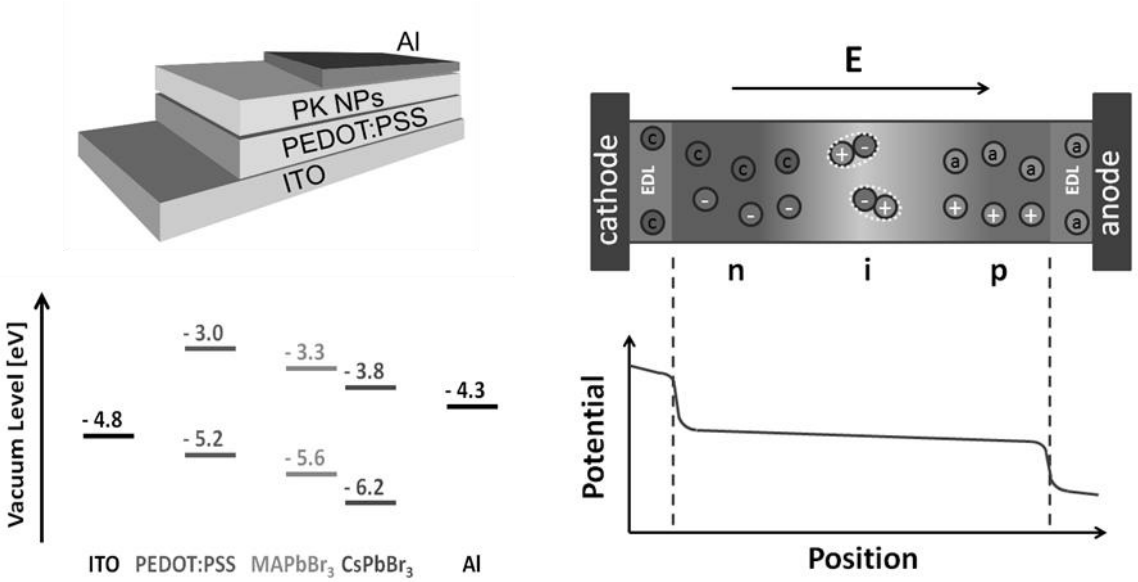

Figure 1. Left – Representative scheme of a LEC device (top) and its approximate energy diagram (bottom). Right – Sketch of the LEC electrochemical doping model with potential profile, in which the electronic (white; - is electron and + is hole) and ionic (black; c is cation and a is anion) carriers are illustrated. EDLs are represented in grey and the non-doped region, where both p- and n-type doped regions (dark grey) merge, is shown in light grey.

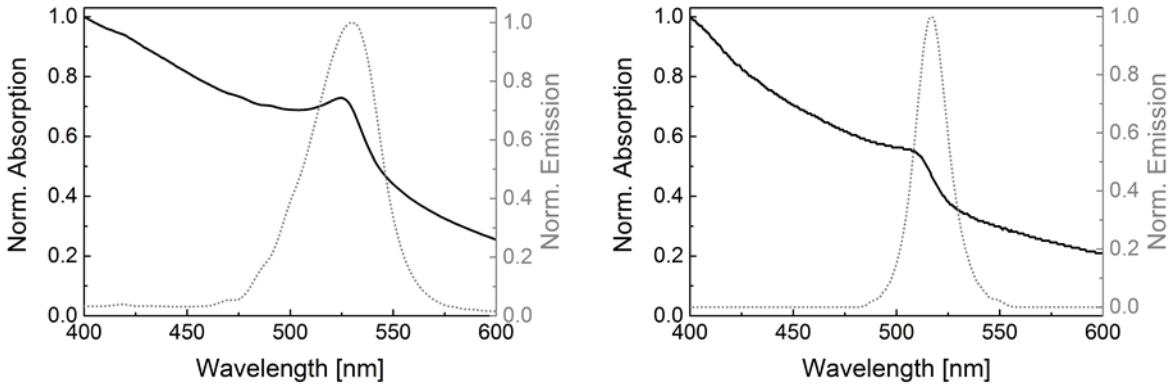

Figure 2. Normalized absorption (black, solid) and emission (grey, dotted) spectra at an excitation wavelength of 350 nm of MPK NP (left) and CPK NP (right) films.

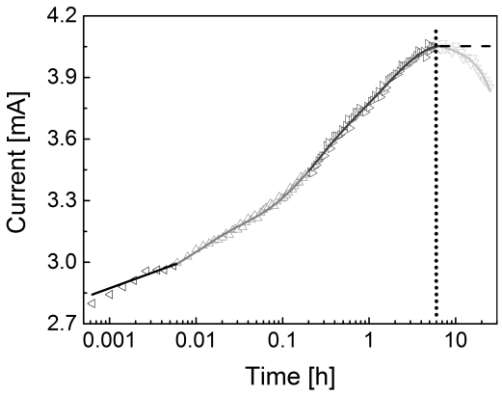

Figure 3. Current density as a function of time of MPK NP devices driven at constant voltage of 4 V. The shading code represents the three formation processes, namely the EDL with halide (black, ◄) and imbalance in the electrode potentials and/or organic cation diffusion (grey, ▲), the growth of charge carrier doped layers (dark grey, ►), as well as degradation of the device (light grey, ▼), which starts from the dotted line onwards. The fitting is given in solid lines. The dashed line demonstrates the run of the curve that is expected for a degradation-free device.

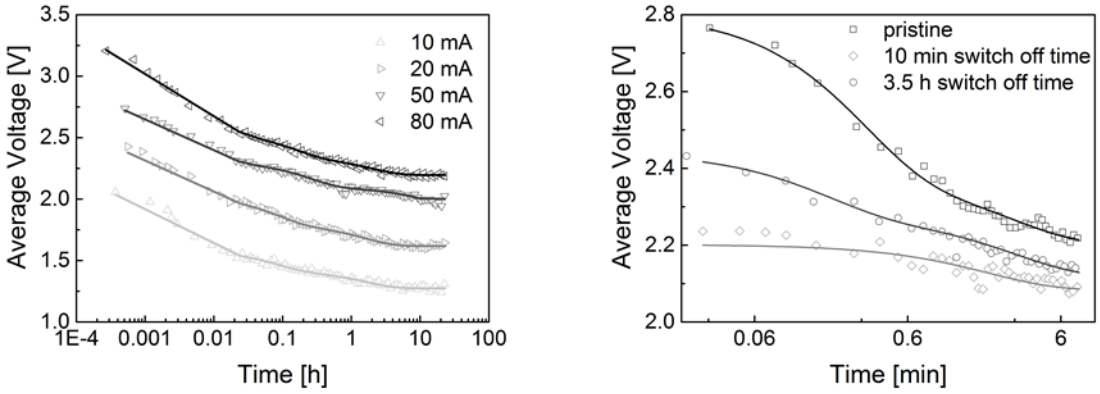

Figure 4. Left – Average voltage as a function of time of ITO/PEDOT:PSS/MPK NP/Al driven at four different pulsed currents of 10, 20, 50, and 80 mA with tri-exponential fits (solid line). Right – Average voltage as a function of time of ITO/PEDOT:PSS/MPK NP/Al driven at a pulsed current of 50 mA during a period of 8 min before and after a switch off time of 10 min or 3.5 h with bi-exponential fits for pristine devices and the biased device after 3.5 h switch off time, as well as mono-exponential fit for the biased device after 10 min switch off time. Fits are given as solid line.

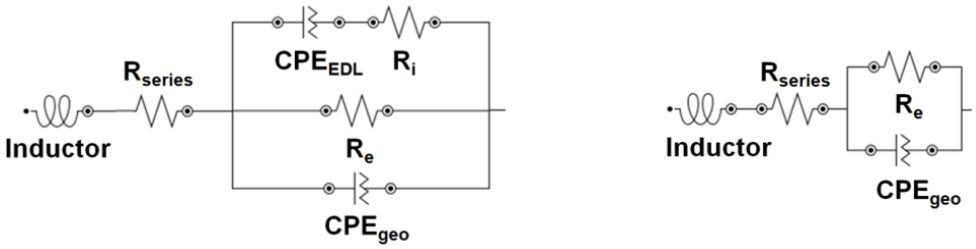

Figure 5. Left – Circuit model with EDL related capacitance (CPE_{EDL}), ionic resistance (R_i), electrical resistance (R_e), and geometric capacitance (CPE_{geo}) used for dynamic EIS assays. Right – Simplified circuit model with only electrical resistance (R_e) and geometric capacitance (CPE_{geo}) used for static EIS assays. In both, series resistor (R_{series}) and inductor elements for the cables were also used.

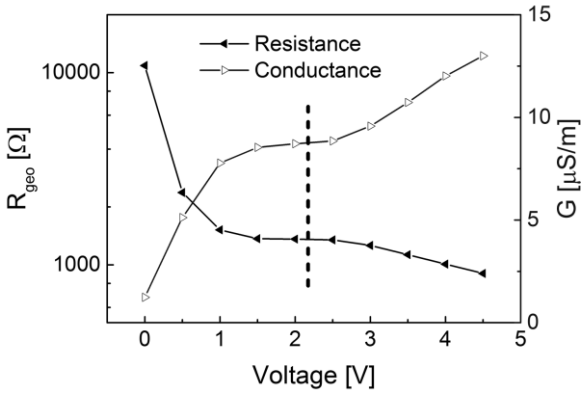

Figure 6. Resistance (filled triangles) and conductance (empty triangles) as a function of voltage for the MPK NP device. The band gap of the material is indicated with a dashed line.

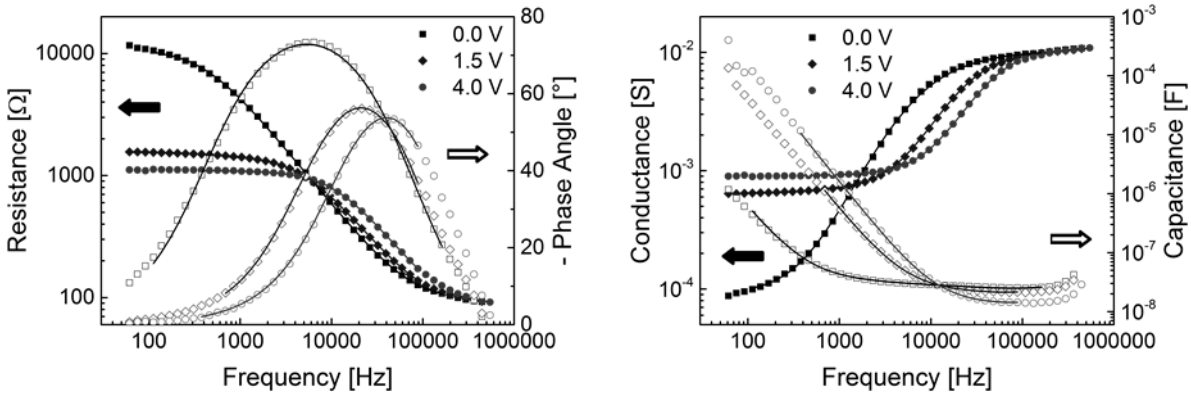

Figure 7. Frequency-dependent resistance and phase angle (left) and corresponding capacitance and conductance (right) of MPK NPs at 0 V (squares), 1.5 V (diamonds), and 4 V (circles). The fitting is given as solid lines.

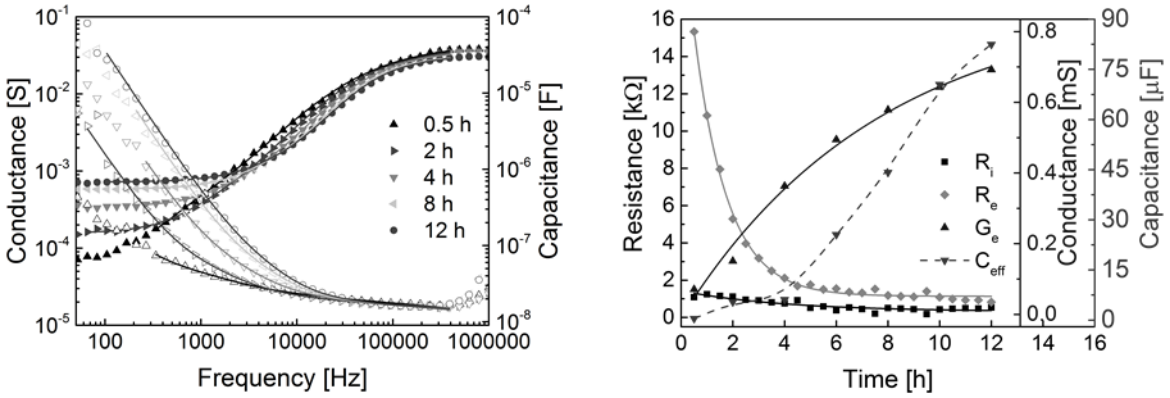

Figure 8. Left part - Frequency-dependent capacitance and conductance of MPK NP devices at 0.5, 2, 4, 8, and 12 h during a constant applied potential of 3 V. The inset illustrates the circuit model used for the fitting that is given as solid lines. Right part - Electric characterization of MPK NP devices as a function of time, with the ionic resistance (black square), electric resistance (light grey diamond), conductance (dark grey ▲), and effective capacitance (grey ▼). The fittings are given as solid lines.

Table 1. Time constants of devices driven at different pulsed currents.

Type of PK NP	Pulsed current [mA]	τ_1 [sec]	Error ±	τ_2 [min]	Error ±	τ_3 [h]	Error ±
MPK	10	16	0.6	4.9	0.4	1.6	0.1
	20	18	1.0	5.1	0.3	1.5	0.1
	50	21	1.1	4.2	0.5	1.1	0.1
	80	15	0.5	5.4	0.2	1.6	0.1
CPK	10	10	0.8	12.0	2.3	-	-
	20	6	0.2	8.1	0.2	-	-

Table 2. Time constants of devices driven at a pulsed current of 50 mA after different switch off times.

Type of PK NP	switch off time	τ_1 [sec]	Error ±	τ_2 [min]	Error ±
MPK	0 sec (fresh)	18	1.0	2.9	0.3
	10 min	-	-	2.0	0.2
	3.5 h	10	1.0	3.0	0.2
CPK	0 sec (fresh)	11	0.7	4.9	0.5
	10 min	11	1.0	1.8	0.1
	3.5 h	35	10.1	57	20

The effect of the ion motion on the mechanism of hybrid perovskite nanoparticles devices is investigated by static and dynamic electrochemical impedance spectroscopy and different poling schemes. We noted a similar behavior to that of light-emitting electrochemical cells, showing three interconnected processes related to the formation of i) electrical double layers at the electrodes' interfaces, ii) the doped regions upon injection, and iii) the non-doped region.

Keywords: perovskite nanoparticles, ionic-based devices, electrochemical impedance spectroscopy, light-emitting electrochemical cells

Bianka M. D. Puscher,[1] Meltem F. Aygüler,[2] Pablo Docampo,[2*] Rubén D. Costa[1*]

Unveiling the Dynamic Processes in Hybrid Lead Bromide Perovskite Nanoparticle Thin Film Devices

ToC figure

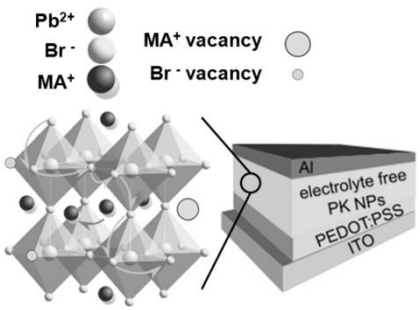

Supporting Information

Unveiling the Dynamic Processes in Hybrid Lead Bromide Perovskite Nanoparticle Thin Film Devices

Bianka M. D. Puscher,[1] Meltem F. Aygüler,[2] Pablo Docampo,[2] Rubén D. Costa[1*]*

Bianka M. D. Puscher and Dr. Rubén D. Costa
Department of Chemistry and Pharmacy, University of Erlangen-Nuremberg (FAU),
Egerlandstr. 3, D-91058 Erlangen, Germany
E-mail: ruben.costa@fau.de
Meltem F. Aygüler and Dr. Pablo Docampo
Department of Chemistry and Center for Nanoscience, University of Munich (LMU),
Butenandtstr. 11, D-81377 Munich, Germany
E-mail: Pablo.docampo@cup.lmu.de

1. Analysis of the Poling Scheme

The tri-exponential fitting used for the analysis of the poling scheme is

$$y = y_0 + A_1 e^{\left(-\frac{x-x_0}{t_1}\right)} + A_2 e^{\left(-\frac{x-x_0}{t_2}\right)} + A_3 e^{\left(-\frac{x-x_0}{t_3}\right)} \quad (1)$$

2. Electrochemical Impedance Spectroscopy

Generally speaking, a small alternating voltage (v_{ac}) is applied and the resulting current response (i_{ac}) and its phase shift (ϕ) compared to the voltage is recorded. By varying the frequency (ω) of the perturbation, the charge carriers in different parts of the device are affected. The parameters obtained by the measurements are composed of a real part and an imaginary part according to

$$\frac{1}{Z} = \frac{i_{ac}}{v_{ac}} = |\Delta Z| e^{i\varphi} = G(\omega) + i\omega C(\omega) \quad (2)$$

where ω, Z, G, and C represent the angular frequency, the impedance, the conductance, and the capacitance of the system, respectively. During fitting, the capacitance had to be replaced with a constant phase element (CPE), which is the equivalent electrical circuit component that models the behavior of an imperfect capacitor. This is assumed to be caused by non-uniform

current density distribution and/or reaction rates along the electrode surface, usually caused by an inhomogeneous surface.[1,2] The CPE's impedance is defined as

$$Z_{CPE} = \frac{1}{Q(i\omega)^{\alpha}} \quad (3)$$

where Q, which corresponds to 1/|Z| at ω = 1 rad/s, and α ($0 \leq \alpha \leq 1$) represent no direct meaningful physical value, however, the CPE acts as pure resistor for α = 0 and pure capacitor for α = 1. The effective capacitance for other values of α can be derived by the method of Brug *et al.* with the equation[2]

$$c_{eff} = Q^{1/\alpha} R^{(1-\alpha)/\alpha} \quad (4)$$

3. Method of calculating the ionic conductivity and dielectric constant from the EIS assay

Both ionic conductivity and dielectric constant can be calculated from the EIS assays. Circuits representing the device setup are given in Figure 5. There are for both PK materials two resistances at two different frequencies – Figure 7 and S9. R_{series} (> 200 kHz) is independent on the applied voltage with a typical value of 93.8±2.1 and 86.8±3.9 Ω for $MAPbBr_3$ (MPK NP) and $CsPbBr_3$ (CPK NP) nanoparticle devices, respectively. The other circuits are R_i for the resistance of the ion diffusion and CPE_{EDL} as the capacitance caused by the redistribution of ions at the electrodes, hence both circuits are related to the EDL formation. R_e and C_{geo} correspond to the electrical resistance and the geometrical capacitance, respectively. The full circuit in Figure 5 (left) was used for dynamic and the simplified circuit in Figure 5 (right) for static EIS, as described in the main text.

The conductivity (σ) of the perovskite nanoparticle films is calculated by using the ionic conductance estimated from Figure 7 and S9 (right) as well as the formula

$$\sigma = \frac{GL}{A} \quad (5)$$

where L (100 nm and 200 nm for MPK and CPK NP, respectively) is the thickness of the active layer and A = 15 mm² the active area of the device. The dielectric constant (ε_r) can be determined with

$$C = \frac{\varepsilon_0 \varepsilon_r A}{L} \quad (6)$$

where C is the effective capacitance and ε_0 the vacuum permittivity (8.85 x 10^{-12} F/m).

In Figure 6 and S9, R_{geo} was taken from the fitting and the ionic conductance from the frequency-dependent conductance in the low frequency regime – Figure S6.

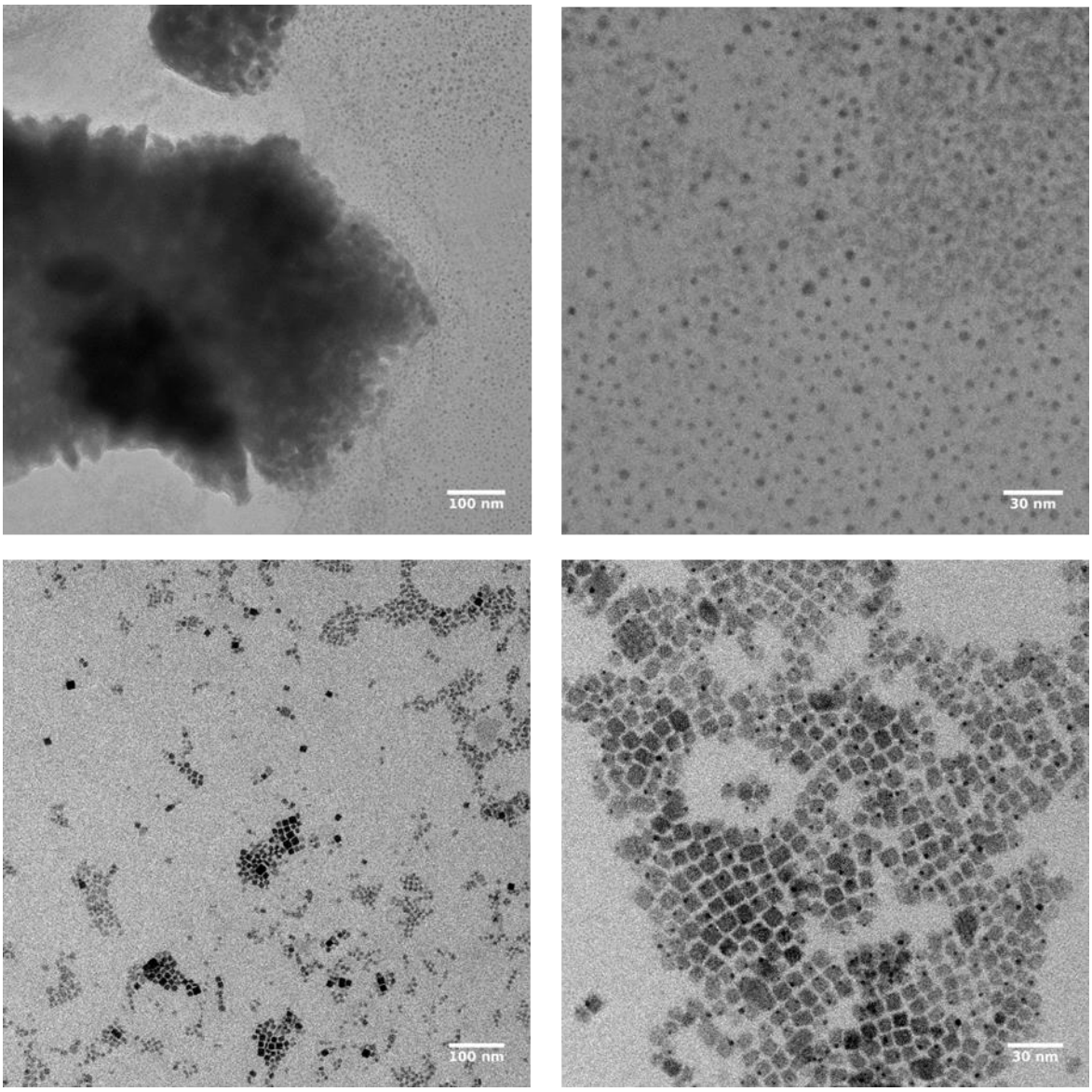

Figure S1. TEM images of MPK (top) and CPK (bottom) at different scale bars of 100 nm (left) and 30 nm (right).

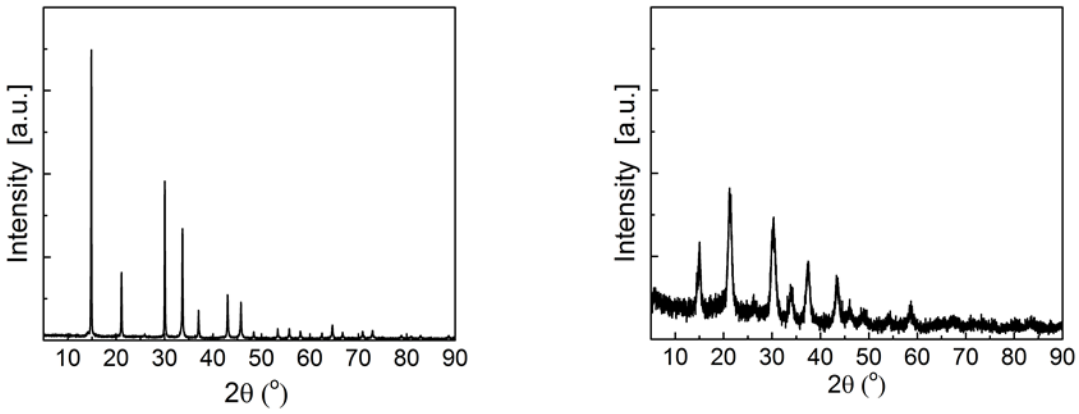

Figure S2. XRD spectra of MPK (left) and CPK (right) NP powder.

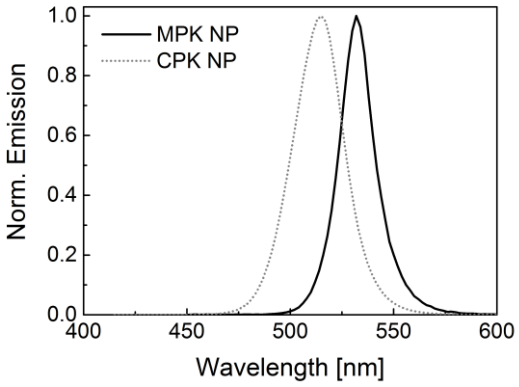

Figure S3. Normalized emission spectra at an excitation wavelength of 405 nm of MPK (black solid) and CPK (grey, dotted) NP dispersions in THF and hexane, respectively.

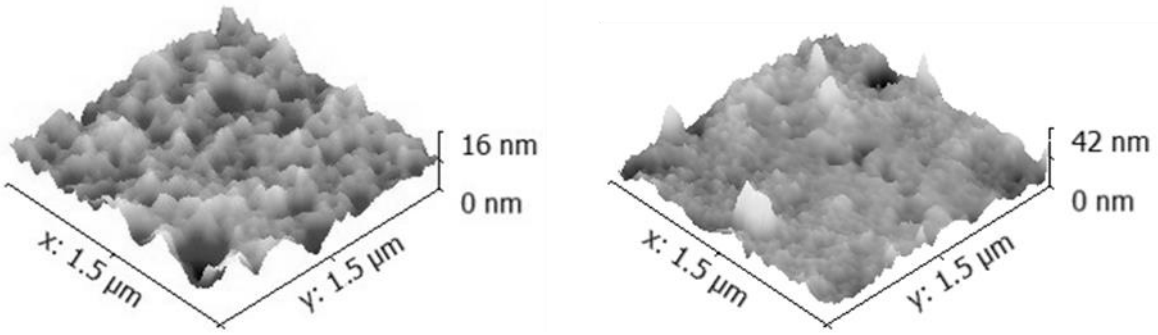

Figure S4. AFM image of MPK (left) and CPK (right) NP films.

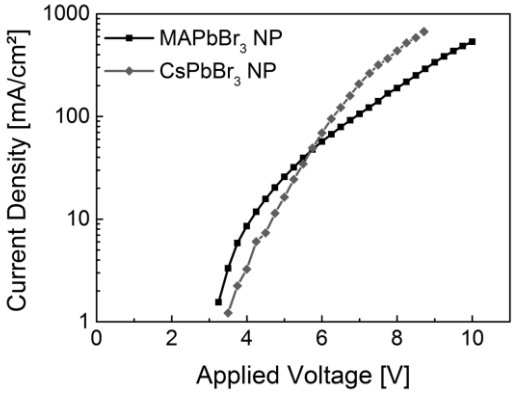

Figure S5. Current density as a function of applied voltage of ITO/PEDOT:PSS/PK NP/Al, with MPK NP (black square) and CPK NP (grey diamond).

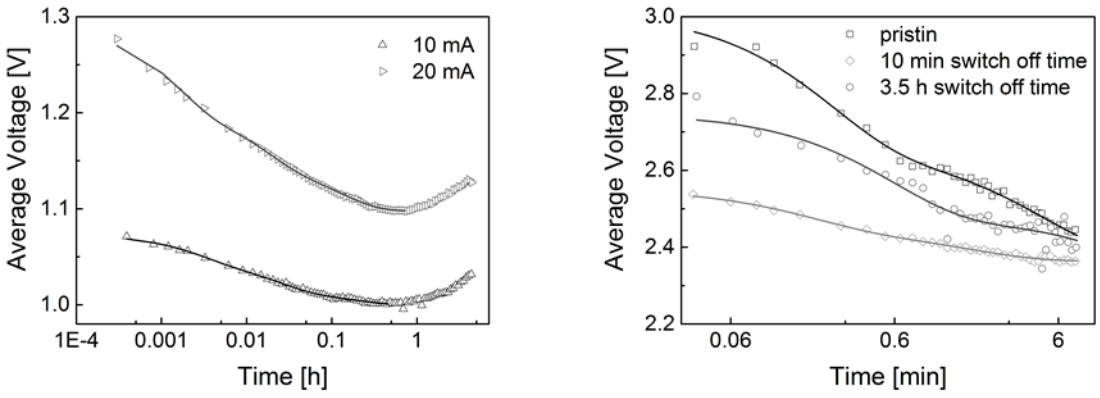

Figure S6. Left – Average voltage as a function of time of ITO/PEDOT:PSS/CPK NP/Al driven at two different pulsed currents of 10 and 20 mA with bi-exponential fits (solid line).

Right – Average voltage as a function of time of ITO/PEDOT:PSS/CPK NP/Al driven at a pulsed current of 50 mA during a period of 8 min before and after a switch off time of 10 min and 3.5 h with bi-exponential fits.

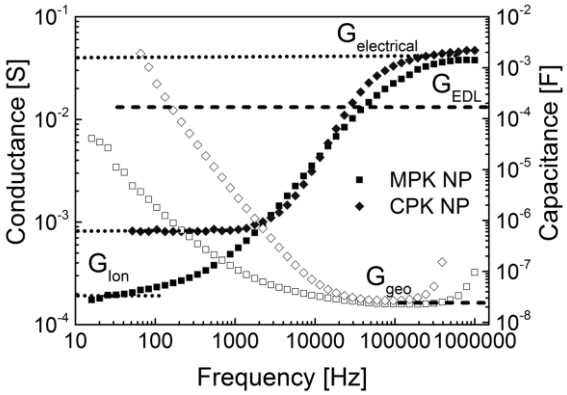

Figure S7. Frequency-dependent conductance (filled) and capacitance (empty) of MPK NP (square) and CPK NP (diamond) at 0 V.

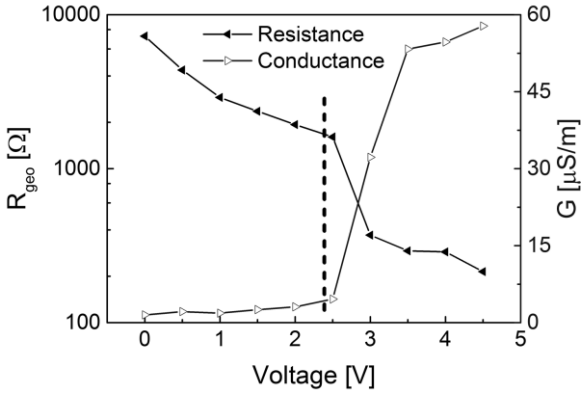

Figure S8. Resistance (filled triangles) and conductance (empty triangles) as a function of voltage for CPK NP (right) devices. The band gap of the material is indicated with a dashed line.

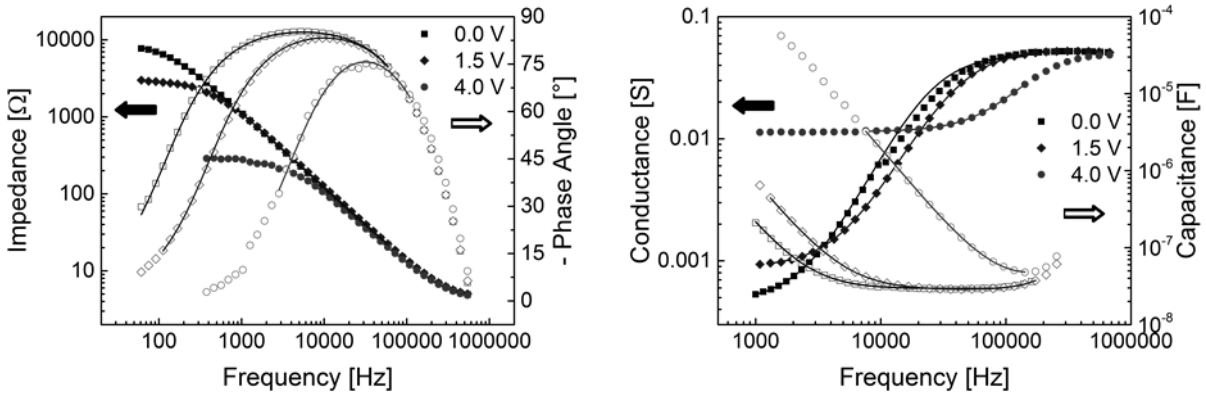

Figure S9. Frequency-dependent resistance and phase angle (left) and corresponding capacitance and conductance (right) of CPK NPs at 0 V (squares), 1.5 V (diamonds), and 4 V (circles). The fitting is given as solid lines.

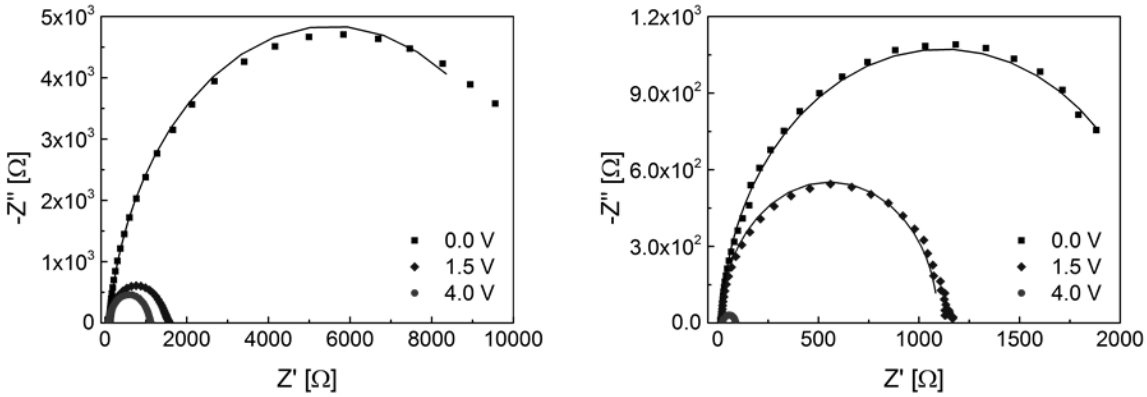

Figure S10. Nyquist plots of impedance spectra of MPK NP (left) and CPK NP (right) at 0 V (squares), 1.5 V (diamonds), and 4 V (circles). The fitting is given as solid lines.

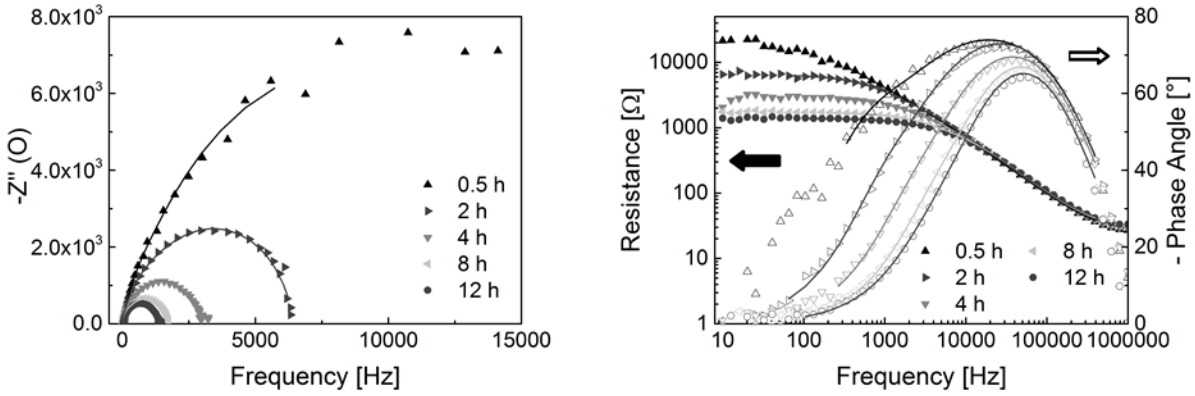

Figure S11. Nyquist and Bode plots of MPK NP during constant applied potential of 3 V at 0.5, 2, 4, 8, and 12 h.

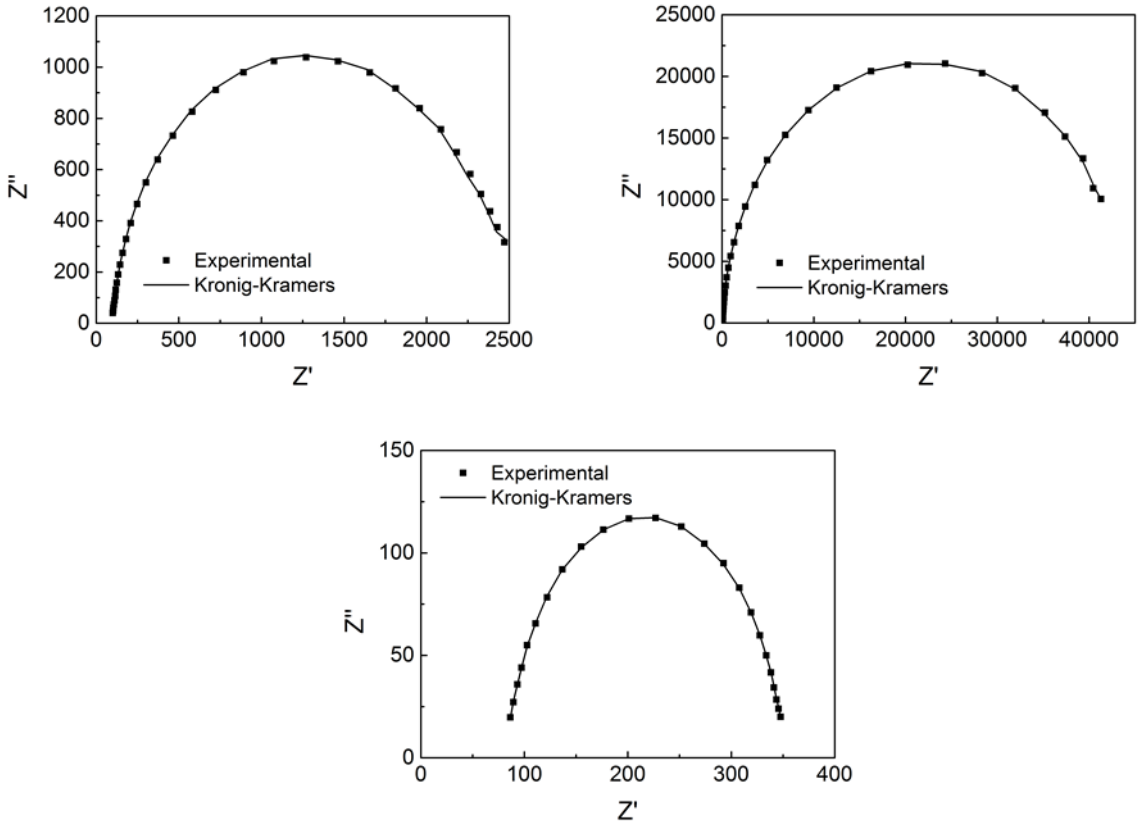

Figure S12. Comparison between experimental and Kronig-Kramers transformation data of MPK (top, left) and CPK (top, right) NP-based film devices at 0 V in a static mode EIS assay, as well as of a MPK NP-based film device at 3 V after 30 min in a dynamic mode EIS assay (bottom).

Table S1: Resulting Parameters of Kronic-Kramer transformation.

Type	Mode	Z'	Z''
MPK	Dynamic (3 V)	1.7×10^{-6}	2.7×10^{-6}
	Static (0 V)	6.0×10^{-5}	5.0×10^{-5}
CPK	Static (0 V)	2.5×10^{-6}	4.1×10^{-6}

(1) Meier, S. B.; Hartmann, D.; Winnacker, A.; Sarfert, W.. *J. Appl. Phys.* **2014**, *116*, 104504.
(2) Brug, G. J.; van den Eeden, A. L. G.; Sluyters-Rehbach, M.; Sluyters, J. H. *J. Electroanal. Chem. Interfacial Electrochem.* **1984**, *176*, 275.